

Combined Feedforward/Feedback Control of Atomic Force Microscopes

Lucy Y. Pao, Jeffrey A. Butterworth, and Daniel Y. Abramovitch

Abstract—The Atomic Force Microscope (AFM) is a powerful imaging and nanofabrication tool that allows the user to observe and manipulate samples at the atomic level. However, one limitation of current AFMs is the long time required to obtain a quality image of a sample. Several researchers have investigated this problem in recent years, and we give an overview of the approaches explored, including H_∞ , ℓ_1 , and model-inverse based methods. We compare and discuss advantages and disadvantages of the various approaches, and we end with a summary of open questions to be addressed in improving the control of AFMs.

I. INTRODUCTION

Atomic Force Microscopy (AFM) can provide images with resolution at the atomic scale (10^{-10} m). In terms of resolution, cost, imaging environments allowable, and ease of sample preparation, AFM has advantages over other microscopy techniques such as tunneling electron microscopy (TEM), scanning electron microscopy (SEM), and optical imaging methods. However, the quality and speed of AFM images depend upon the overall dynamics of the AFM system. The behavior of AFMs varies considerably across AFM tips as well as changes in samples and environmental changes. Currently, the variability causes commercial AFMs to not behave like reliable instruments, and this slows down and frustrates AFM users. The overall dynamics of AFMs can be improved by improving either the dynamics of the actuators themselves or by improving the control system. Further background on AFMs can be found in [1] and the references therein, and methods for improving the mechanics of AFMs through redesign of the actuators are discussed in [29]. In the current paper, we will overview several combined feedforward/feedback control methods for AFMs.

A schematic diagram of a piezoscanner-based positioning of the AFM probe, relative to the sample surface, is shown in Fig. 1, and a block diagram showing a combined feedforward/feedback architecture for controlling an AFM is presented in Fig. 2. The AFM operation process is initiated by gradually reducing the distance between the AFM probe and the sample (by using a piezo actuator) until a prespecified probe-sample interaction is achieved, i.e., the AFM cantilever

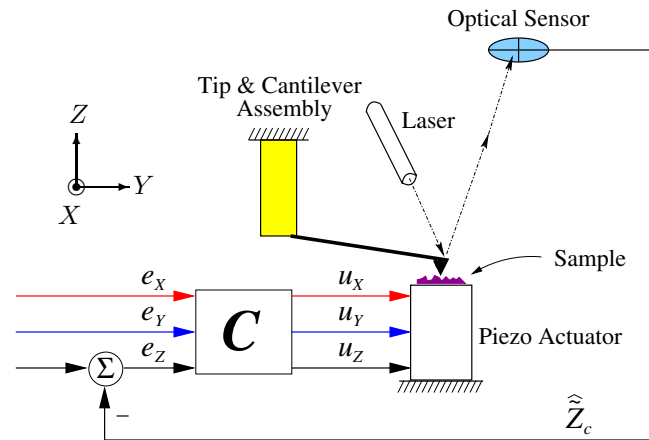


Fig. 1. Schematic diagram of AFM operation. The piezoscanner enables positioning of the AFM probe both parallel (along the X and Y axes) and perpendicular (along the Z axis) to the sample surface.

deflection error \tilde{Z}_c reaches a specified setpoint value $\tilde{Z}_{c,d}$. The AFM cantilever deflection error (which depends on the probe-sample interaction) can be measured using an optical sensor as shown in Fig. 1. Currently, most AFMs use a single-input single-output (SISO) feedback controller to maintain a desired AFM cantilever deflection error as the AFM probe is moved by piezo actuators to scan the sample surface. The scanning movement is a rastering (back and forth) movement of the AFM probe relative to the sample in the X direction while the Y position is incremented, and most AFMs currently only use feedforward control for the X and Y directions. The X -direction motion is the fast scan direction, while motion in the Y direction is much slower. The Z -direction motion control is carried out depending upon the amount of cantilever deflection, which depends upon the topology of the sample.

There are several variations in AFM designs in terms of whether the tip and cantilever assembly are actuated and/or the sample stage is actuated. In one typical scanning sample design, the sample is moved below a stationary tip, and the X , Y , and Z actuation are done by a single piezo tube actuator [7]. In a scanning tip design, the sample is stationary while the tip is moved in X , Y , and Z . In a third design, the X - Y motion is handled by a stage that moves the sample while the Z motion is handled by an actuator moving the cantilever up and down. The choice of designs depends greatly on the type of AFM measurement to be done, and the issues are discussed further in [16], [29].

Non-raster scan methods are not very common, but have recently been explored and show significant advantages for

This work was supported in part by Agilent Technologies, Inc. and the US National Science Foundation (NSF Grant CMS-0201459). The authors thank Brian P. Rigney for his comments and suggestions for this paper.

L. Y. Pao is a professor of Electrical and Computer Engineering at the University of Colorado at Boulder, Boulder, CO 80309 USA, pao@colorado.edu

J. A. Butterworth is a graduate student of Electrical and Computer Engineering at the University of Colorado at Boulder, Boulder, CO 80309 USA, butterwo@colorado.edu

D. Y. Abramovitch is a senior research engineer in the Nanotechnology Group at Agilent Laboratories, 5301 Stevens Creek Blvd., M/S: 4U-SB, Santa Clara, CA 95051 USA, danny@agilent.com

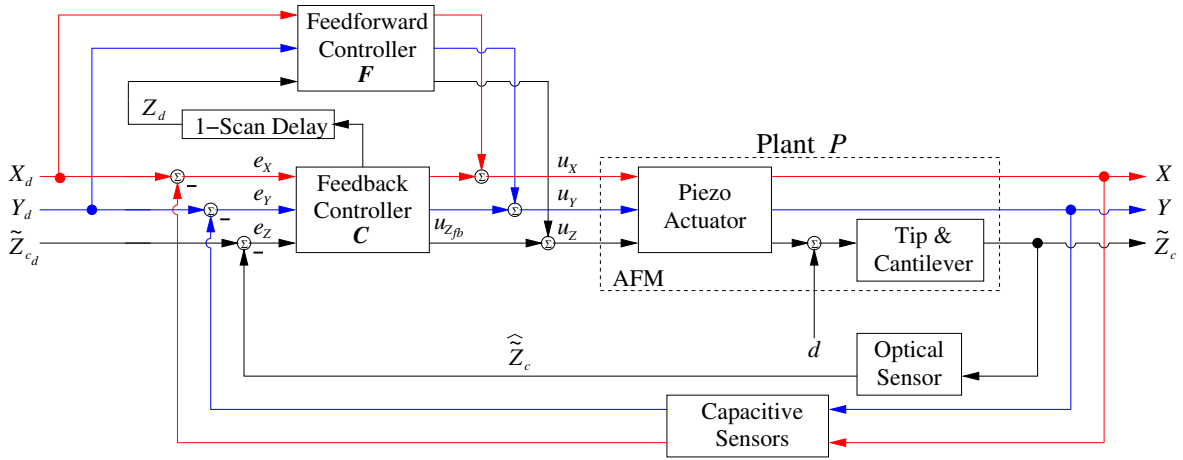


Fig. 2. Block diagram of a combined feedforward/feedback architecture for controlling an AFM, consisting of the feedback compensator C and a feedforward controller F . In addition to the reference signals into the loop, the actuator signals into the plant can be altered to improve performance.

imaging string-like samples such as nanowires or DNA strands [2], [3]. In these non-raster scan methods, the scan control algorithm steers the AFM tip around a particular area of interest. Generally, this area of interest is determined using the information from previous sample points. Thus, these methods determine which points to sample in a closed-loop, rather than open-loop method. This allows the scan algorithm to concentrate measurement points around the area of interest, rather than evenly distribute them over the entire sample. In the standard method, the majority of the measurement points are likely in areas of little interest. A survey of non-raster scan methods, with a discussion of how they may be applied to AFMs is given in [4]. While the typical raster scanning is assumed in discussing control methods in this paper, these control techniques can generally also be applied to non-raster scan trajectories.

In AFM imaging in *constant-force mode*, the control goal is to regulate the AFM cantilever deflection error \tilde{Z}_c at a constant value (the setpoint value $\tilde{Z}_{c,d}$, which is often zero). Large variations in the AFM cantilever deflection error \tilde{Z}_c can cause sample damage (or AFM probe damage). Variations in the setpoint value of the cantilever deflection error $\tilde{Z}_{c,d}$ may be required, however, to manipulate or modify a sample, e.g., to indent a sample during nanofabrication. This paper generally assumes constant-force mode, as opposed to dynamic or AC mode operation of AFMs [1], [14], [15].

Since the time required to attain a quality AFM image is typically on the order of several minutes or more, substantial motivation exists to speed up the imaging time in AFMs. Faster imaging is required to capture and explore the dynamics of biological samples [10], [32] and improved speed is also necessary for nanofabrication to be economically viable.

In this paper, we overview and compare a number of control methods that have been developed for AFMs in Section II. Simulation results of these methods as applied to the X -axis control loop are then presented in Section III. A model of a nPoint (www.npoint.com) NPXY100A stage is used, where the model is extracted based on measurements

of an actual stage. These examples demonstrate the application of several control methods to a model of a physical system. We then discuss the state of the field and future work for further improving the control of AFMs in Section IV.

II. CONTROL OF AFMS

A block diagram of a combined feedforward/feedback architecture for controlling an AFM is shown in Fig. 2. A similar architecture can be used for many applications. In Fig. 2, the dynamics of the AFM piezo actuator and tip and cantilever are represented in the AFM block. The piezo actuators in the X , Y , and Z directions move the piezo scanner in these directions. d is the surface of the sample being imaged, and since it is yet unknown, d acts as a disturbance to the AFM. The sample surface causes the cantilever to deflect, the deflection error \tilde{Z}_c is measured by an optical sensor, and the result is fed back to the controller C . Some AFMs have capacitive, strain gauge, or LVDT sensors that measure the X and Y positions for feedback [23], [31]; and some AFMs do not have such sensors and the X and Y directions are not controlled in a feedback loop.

In current AFMs, C is typically a diagonal matrix

$$C(w) = C_0(w) = \begin{bmatrix} C_X(w) & 0 & 0 \\ 0 & C_Y(w) & 0 \\ 0 & 0 & C_Z(w) \end{bmatrix} \quad (1)$$

consisting of a scalar dynamic feedback controller for each direction, and where w denotes a complex frequency. The discussion here can be carried out in terms of either continuous- or discrete-time controller design. Since controllers are typically implemented digitally, we will generally assume discrete-time controllers, with $C(w)$ indicating the z -transform transfer function of the controller. When X and Y are not measured, C is as in (1) with $C_X(w) = C_Y(w) = 0$:

$$C(w) = C_{0z}(w) = \begin{bmatrix} 0 & 0 & 0 \\ 0 & 0 & 0 \\ 0 & 0 & C_Z(w) \end{bmatrix}. \quad (2)$$

F is a feedforward compensator that can alter the actuator commands to the AFM. Thus far in the AFM literature, F has taken on the form

$$F(w) = F_0(w) = \begin{bmatrix} F_X(w) & 0 & 0 \\ 0 & 0 & 0 \\ 0 & 0 & F_Z(w) \end{bmatrix}. \quad (3)$$

Assuming a linear, time-invariant (LTI) plant model, as has often been done in the literature, the AFM plant is multi-input multi-output (MIMO) of the form

$$P(w) = \begin{bmatrix} P_{XX}(w) & P_{XY}(w) & P_{XZ}(w) \\ P_{YX}(w) & P_{YY}(w) & P_{YZ}(w) \\ P_{ZX}(w) & P_{ZY}(w) & P_{ZZ}(w) \end{bmatrix} \quad (4)$$

where $P_{XX}(w)$ represents the transfer function from the X -axis control input to the X position, $P_{XY}(w)$ represents the transfer function from the Y -axis control input to the X position, $P_{XZ}(w)$ represents the transfer function from the Z -axis control input to the X position, and so forth. Due to coupling effects, $P(w)$ is a full matrix. P_{XY} , P_{YX} , P_{YZ} , and P_{ZY} are generally relatively small compared with the other entries [31], [36]. The cross-coupling between the X and Z directions, however, can be significant [36].

The cross-coupling in AFMs can be more or less severe depending upon whether a tube actuator or a separate X - Y scanner is used. With a tube actuator, there is coupling due to the structure with piezos on the outside for the X and Y motion and a piezo on the inside for the Z motion [1]. One way to minimize the coupling is to minimize the scan area, since as the area shrinks, the angle of the piezo actuator pendulum remains small leading to better decoupling. Approximately $25 \text{ nm} \times 25 \text{ nm}$ or smaller is a small scan area. However, large scan areas (of $250 \text{ nm} \times 250 \text{ nm}$ or larger) are required for a number of applications, such as imaging biological cells [12], [18], [32], and it is hence very important to be able to adequately decouple the dynamics for high speed and high quality AFM imaging. When there is a separate X - Y scanner, the coupling from the lateral motion into the Z axis is less pronounced. Furthermore, modern external X - Y scanners are designed to specifically decouple the motion of their fast and slow axes by having the X scanner (fast direction) mounted within a frame that is moved in Y (slow direction) by the Y scanner [5], [28], [31]. However, there is still coupling between the X - Y motions and the Z direction through the cantilever and tip dynamics, so as the surface goes back and forth at high speed, there is coupling into the cantilever and hence the optical detection system.

Commercial AFMs are typically controlled with basic Proportional (P), Proportional-Integral (PI), Proportional-Integral-Derivative (PID), Proportional-Double-Integral (PII), or Proportional-Double-Integral-Derivative (PIID) compensators [11], [23], [25], [31], [35]. Here, $F = 0$, and for a PIID feedback controller for the Z motion direction, a continuous-time compensator transfer function is

$$C_Z(s) = \left(K_p + \frac{K_i}{s} + \frac{K_{ii}}{s^2} + K_d s \right) E_Z(s)$$

where $E_Z(s)$ is the Laplace transform of the error signal $e_Z(t)$. For a P, PI, PII, or PID controller, one or more of the K_d , K_i , or K_{ii} gains are set to zero. PIID controllers are typically specified in continuous time, s , and are usually implemented in discrete time, z , typically using an integrator equivalent [6]. However, analog implementations are used in some high bandwidth experiments [5], [28]. Due to noisy measurements and uncertainty in the actuator models, K_d is often set to 0 in AFM systems. The K_p , K_i , K_{ii} , and K_d gains must be tuned carefully to achieve high-bandwidth and good regulation of the cantilever deflection error \tilde{Z}_c near the desired level \tilde{Z}_{cd} . Users of commercial AFMs know all too well that the tuning of the PIID gains is a tedious process, and several control systems researchers have recently shown significant improvements in the speed and quality of AFM images using more advanced controllers discussed below.

A. H_∞ Control

Schitter and others have developed SISO H_∞ feedback controllers [25] for the Z -motion, where a linear controller C_Z is designed to minimize the H_∞ norm of

$$T_{fb} = \left\| \begin{bmatrix} W_e S_Z \\ W_u C_Z S_Z \\ W T_Z \end{bmatrix} \right\| \quad (5)$$

where the sensitivity function is $S_Z = (1 + \hat{P}_{ZZ} C_Z)^{-1}$, the complementary sensitivity function is $T_Z = \hat{P}_{ZZ} C_Z (1 + \hat{P}_{ZZ} C_Z)^{-1}$, \hat{P} is the plant model used for control design, and W_e , W_u , and W are weighting functions that are chosen to yield fast motion control, suppress disturbances, and provide robustness against model uncertainties [34], [40]. In H_∞ control, the worst-case system energy gain is minimized.

Schitter and others have also explored the use of SISO H_∞ feedforward controllers for motion in the X and Z directions [26], [27], where the feedforward filter F_X is designed to minimize the H_∞ norm of

$$T_{ff} = \left\| \begin{bmatrix} W_{u_f} F_X \\ W_{X_f} - W_{X_f} \hat{P}_{XX} F_X \end{bmatrix} \right\| \quad (6)$$

and similarly for the Z direction. W_{u_f} and W_{X_f} are weighting functions that are chosen to yield fast motion control and robustness against model uncertainties. For feedforward control in the X direction, the desired X -direction path in the raster-scanning pattern is fed forward. In the Z direction, the Z topology from the previously scanned line is used in determining the feedforward signal, as indicated in Fig. 2.

H_∞ designs often lead to high-order controllers, though relatively high-order controllers can generally be accommodated in AFMs, as they are advanced instruments that usually are not extremely limited computationally. Schitter and his collaborators have been able to show improvements in speed (up to 15 times faster) and quality (down to $\frac{1}{6}$ the variations in cantilever deflection levels) in various experiments when compared to traditionally tuned PI-type controllers.

S. Salapaka and M. Salapaka and their groups have also explored SISO H_∞ feedback control of AFMs [23], [24],

[30], [31], where in Fig. 2, $F = 0$ and C is as in (1) with C_X , C_Y , and C_Z designed as discussed in (5), yielding higher speed and higher quality images than PI controllers. They have also shown that their H_∞ feedback controller designs virtually eliminate hysteretic and creep effects in the piezo actuator. In [31], they also apply the Glover-McFarlane H_∞ design [13], [17] to improve the robustness of existing PII designs. Since the control signal for the Z -actuator is often used to compute the sample profile [1], the H_∞ feedback control law in [24] is designed also to enable an accurate profile estimate signal in the presence of modeling errors.

B. ℓ_1 Control

Stemmer and others have reported faster and more accurate imaging results using SISO ℓ_1 -optimal feedback and feedforward controllers [20], [35] for the vertical (Z -direction) scanner position. In the ℓ_1 framework, the goal is to minimize the maximum or peak deviations of signals. The feedback compensator C_Z consists of an ℓ_1 controller, C_{Z_1} , in cascade with a filter, C_{Z_2} , that is included to smooth the open-loop gain. The minimization in ℓ_1 -optimal control takes place in the time domain, and C_{Z_1} is designed to minimize the weighted cantilever deflection error \hat{Z}_c and the controller output signal $u_{Z_{fb}}$. The ℓ_1 -optimal feedforward controller F_Z is designed to minimize the weighted tracking error, where as with the H_∞ feedforward controller discussed above, the previous recorded scan line is used in computing the feedforward reference trajectory.

C. Model-Inverse Based Control

Devasia and others have studied model-inverse methods for AFMs [8], [9], [36], [39], [41], where C is as in (2) with C_Z being a PID or other controller, and F is as in (3) where

$$F_X \approx \hat{P}_{XX}^{-1} \quad \text{and} \quad F_Z \approx \hat{P}_{ZZ}^{-1} \quad (7)$$

are designed to be approximate inverses of the corresponding models \hat{P}_{XX} and \hat{P}_{ZZ} of the plant. Due to the flexible structure and non-collocated sensing/actuation nature of the piezo scanner, the plant and its model \hat{P} generally have non-minimum phase zeros. As such, \hat{P}_{XX}^{-1} and \hat{P}_{ZZ}^{-1} are unstable, and stable approximate inversions have been developed and used by Devasia and his collaborators. Other researchers have also investigated approximate model-inverse control methods for nonminimum phase systems in other application areas [19], [37], [38]. Devasia and his colleagues have shown that model-inverse based approaches as in (7) are effective in AFMs at compensating for loss of precision due to hysteresis during long range applications, due to creep effects during positioning over extended periods of time, and due to induced vibrations during high-speed positioning. They have also used model-inverse based feedforward compensation and iterative learning control (ILC) methods to compensate for hysteresis and to mitigate the effects of coupling between the X - and Z -axes of motion [36], [39]. While ILC methods can be effective for repetitive motions, such as the raster scanning in AFMs, they do not apply to non-repetitive motions such as would occur with non-raster scanning techniques [4]. ILC

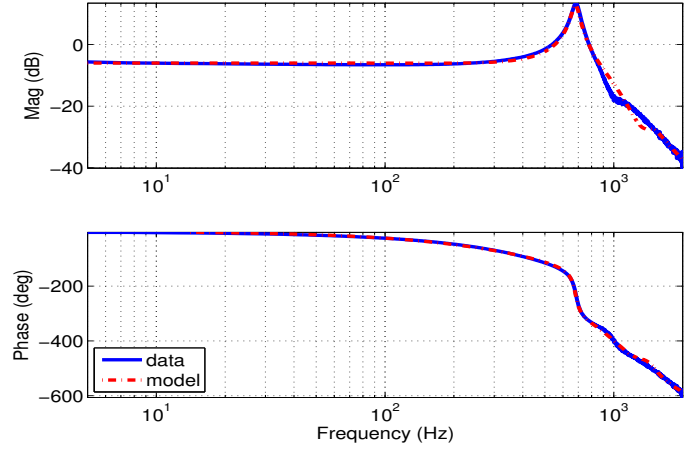


Fig. 3. Frequency response functions characterizing the plant for motion in the X direction. The plant model has been extracted based upon the measurement data shown of an actual X - Y stage.

methods also require a number of iterations for convergence when the desired trajectory to be followed changes, as happens in the Z direction in AFMs.

III. COMPARISON OF CONTROL APPROACHES

While several of the advanced control approaches have been shown to yield significantly improved performance, no direct comparisons between these approaches have been made. In this section, we provide a comparison of a few of the control methods overviewed in Section II. A model for motion in the X direction of an nPoint X - Y stage will be used for the control designs. Based upon the frequency response function shown in Fig. 3, we obtain the following 7th-order discrete-time transfer function model

$$\hat{P}_{XX}(z) = \frac{-0.0014(z - 0.0061)(z - 1.7824)}{(z - 0.8884)(z - 0.8572 \pm j0.4032)} \times \frac{(z - 1.1264 \pm j0.4627)(z - 0.8762 \pm j0.3766)}{(z - 0.8717 \pm j0.2742)(z - 0.9716 \pm j0.2022)}. \quad (8)$$

There are three nonminimum phase zeros that pose some challenges in the control design. All the controllers are designed and implemented with a sample rate of 20.833 kHz.

A reasonably-tuned PID controller of the form given by C_{PID} in Table I yields the performance shown in Fig. 4 of a 100 Hz back-and-forth motion. The negative proportional gain in C_{PID} is due to a constraint imposed by nPoint's controller hardware, which we will ultimately be using to do initial experimental evaluations on the X - Y stage. That C_{PID} is a continuous-time controller, and the other controllers in Table I are in discrete-time is also due to the implementation constraints of the nPoint controller hardware.

After some iteration, using the following weights in (5) yields satisfactory H_∞ feedback controller performance:

$$W_e = \frac{4z - 0.9841}{100(z - 1)}, \quad W_u = 0.1, \quad W = \frac{2z - 1.595}{2.024z}. \quad (9)$$

The H_∞ feedback weighting functions were designed in a similar manner to those in [25] and [31]. Specifically, the weight W_e is designed with low-pass qualities. This helps

TABLE I
FEEDBACK AND FEEDFORWARD CONTROLLER DESIGNS.

Controller	Transfer Function	Zeros	Poles
C_{PID}	$-0.05 + \frac{955}{s} + 2.5 \times 10^{-5}s$	$1000 \pm j6099$	0
$C_{H\infty}$	$\frac{2.92z^8 - 15.4z^7 + 31.9z^6 - 27.4z^5 - 4.54z^4 + 31.2z^3 - 28.4z^2 + 11.7z - 1.91}{z^8 - 5.77z^7 + 14.2z^6 - 19.2z^5 + 14.8z^4 - 5.69z^3 + 0.229z^2 + 0.605z - 0.155}$	$-1, 0.8884,$ $0.8572 \pm j0.4032,$ $0.8717 \pm j0.2742,$ $0.9716 \pm j0.2022$	$-0.2956, 1,$ $0.8637 \pm j0.3963,$ $0.9414 \pm j0.3069,$ $0.7252 \pm j0.2581$
$F_{H\infty}$	$\frac{18.5z^6 - 66.1z^5 + 72.1z^4 + 9.54z^3 - 76.9z^2 + 56.3z - 13.5}{z^6 - 1.71z^5 - 0.646z^4 + 2.51z^3 - 0.736z^2 - 0.799z + 0.387}$	$-0.9989, 0.8884,$ $0.8717 \pm j0.2742,$ $0.9664 \pm j0.2118$	$-0.9999, -0.6853,$ $0.8775, 0.7692,$ $0.8719 \pm j0.2744$
F_{MI}	$\frac{719.2z^7 - 4523z^6 + 12390z^5 - 19140z^4 + 18020z^3 - 10340z^2 + 3346z - 472}{2.64z^7 - 10.2z^6 + 16.1z^5 - 13.2z^4 + 5.50z^3 - 0.943z^2 + 0.00555z}$	$0.8884,$ $0.8572 \pm j0.4032,$ $0.8717 \pm j0.2742,$ $0.9716 \pm j0.2022$	$0, 0.5610, 0.0061,$ $0.8762 \pm j0.3766,$ $0.7596 \pm j0.3120$

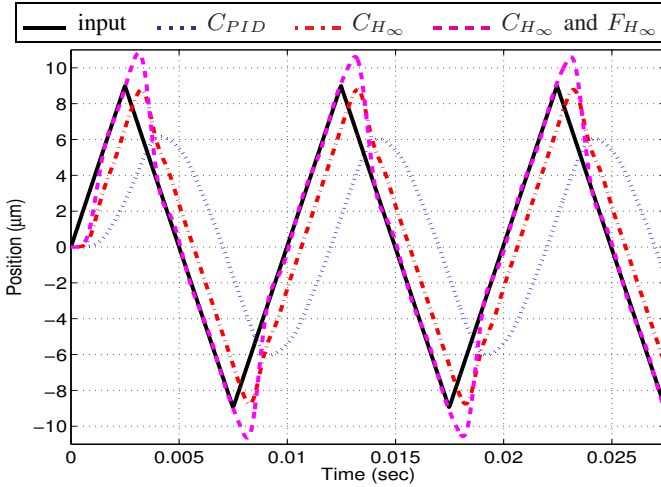


Fig. 4. Simulation results with the PID only (C_{PID}), H_∞ feedback only (C_{H_∞}), and H_∞ feedback and feedforward (C_{H_∞} and F_{H_∞}) controllers.

tracking performance as the resulting sensitivity function will be small at low frequencies. The constant weight W_u is selected to keep the piezo actuator within its saturation limits. Finally, the weight W concerns disturbance rejection and robustness against potential high frequency model uncertainty. It is designed with high-pass qualities which guarantee a rolling-off of the complimentary sensitivity function at high frequencies. The resulting H_∞ feedback controller C_{H_∞} is given in Table I and Fig. 4 shows that the H_∞ feedback controller yields superior tracking of the 100 Hz back-and-forth motion over the PID controller.

Using the following weights

$$W_{u_f} = \frac{0.1334(z - 0.766)(z + 1)}{z^2 - 1.933z + 0.9788}$$

$$W_{X_f} = \frac{2.5z + 4.255}{100(z - 0.9999)} \quad (10)$$

in (6) yields the H_∞ feedforward controller F_{H_∞} given in Table I. These feedforward weights were designed in a manner similar to those in [26], [27]. Here, the weight W_{u_f} was not designed with regard to actuator saturation limits, but rather with regard to the first piezo stage resonance. Since there is often uncertainty in this resonant frequency, the

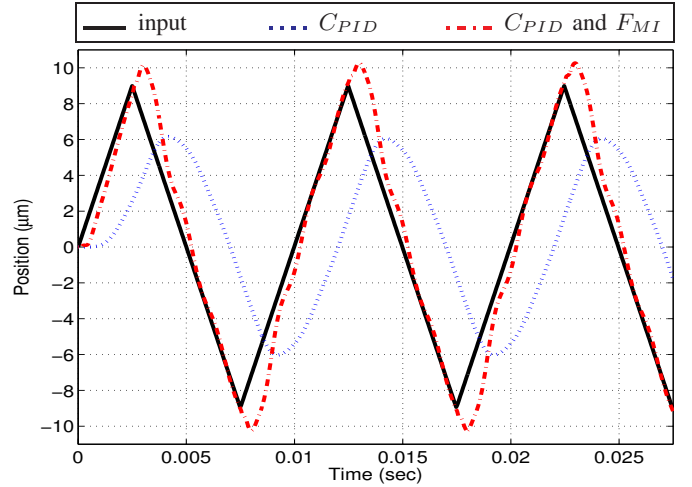


Fig. 5. Simulation results with the PID only (C_{PID}) and the combined PID and model-inverse feedforward (C_{PID} and F_{MI}) controllers.

objective is to avoid exciting the piezo actuator at frequencies near its resonance. In contrast, and similar to W_e , the weight W_{X_f} is designed with low-pass qualities to ensure good reference input tracking. Tracking is not guaranteed at frequencies beyond the bandwidth of W_{X_f} . When using both the feedback and feedforward controllers C_{H_∞} and F_{H_∞} in Table I, Fig. 4 shows that the tracking performance is very good except near the (high-frequency) turnaround points.

Using an approximate model-inversion method [19], [38], we obtained the feedforward controller F_{MI} given in Table I, which when used in conjunction with the PID controller C_{PID} in Table I yields the results in Fig. 5. Compared with the combined C_{H_∞} and F_{H_∞} controller results of Fig. 4, there is less overshooting at the turnaround points, though worse tracking performance away from these turnaround points. While the model-inverse based feedforward controller F_{MI} could also be combined with the H_∞ feedback controller C_{H_∞} , for the particular F_{MI} and C_{H_∞} designs given in Table I, better results were not achieved.

Let us define the following performance measure to quantify the energy in the tracking errors shown in Figs. 4 and 5:

$$J_e = \int \left\{ (X_d(t) - X(t))^2 \right\} dt \quad (11)$$

TABLE II
PERFORMANCE COMPARISON OF VARIOUS CONTROLLERS.

Controller(s)	J_e	J_m
C_{PID}	0.8092	54.0962
$C_{H\infty}$	0.1447	8.3876
$C_{H\infty}$ and $F_{H\infty}$	0.0645	19.1244
C_{PID} and F_{MI}	0.0737	12.6915

where $X_d(t)$ is the reference input signal that $X(t)$ should track. A second performance measure quantifying the (square of the) peak deviation from the desired trajectory is

$$J_m = \max_t \left\{ (X_d(t) - X(t))^2 \right\}. \quad (12)$$

Table II summarizes the tracking performances according to (11) and (12) for the various feedback and combined feedback/feedforward controllers. In terms of J_e , the combined feedback and feedforward controllers perform an order of magnitude better than PID control alone. Further optimization of the H_∞ weights for the $C_{H\infty}$ and $F_{H\infty}$ designs and further optimization of the inversion method used to design F_{MI} could yield similar order-of-magnitude improvements based on the J_m metric as well.

IV. DISCUSSION AND AREAS FOR FUTURE WORK

A number of researchers have explored and applied advanced control methods to AFMs, demonstrating up to an order of magnitude improvements in speed and quality over traditional PID-type controllers. SISO H_∞ feedback and feedforward controllers have been developed to minimize the worst-case energy gain of the system, SISO ℓ_1 feedback and feedforward controllers have been used to minimize the peak errors, and model-inverse based feedforward controllers have shown improved tracking performance.

A brief comparison of H_∞ and model-inversion techniques on a common plant model has been given in Section III. We did not spend a significant amount of time optimizing either the H_∞ or the model-inversion controllers to yield better results based on the performance indices of (11) and (12). By tweaking the H_∞ weights W_e , W_u , W , W_{u_f} , and W_{X_f} , better performing H_∞ controllers $C_{H\infty}$ and $F_{H\infty}$ could be obtained. Indeed, varying the poles and zeros in the weights in (9) and (10) by 1% causes changes of up to 10% in J_e and 26% in J_m ; varying the poles and zeros of the weights by 2% causes changes of up to 53% in J_e and 84% in J_m . This shows the performance sensitivity of the H_∞ controllers to the exact selection of the weighting functions. Similarly, because different model-inversion methods [9], [19], [21], [22], [37], [38], [41] provide varying degrees of dynamic inversion ‘‘accuracy’’ and possible tradeoffs in penalties of noncausal preactuation, exploring different model-inverse methods may lead to better performing F_{MI} controllers. Regardless of the particular method, model-inversion techniques generally yield feedforward F_{MI} controllers of the same order as the plant (7th-order for our plant model). However, depending on how the

various weights are chosen, H_∞ designs can lead to higher-order controllers that may be more difficult to implement.

No ℓ_1 (feedback or feedforward) controllers were designed and compared in Section III. In general, ℓ_1 optimal control theory is less mature and less widely used than H_∞ and model-inverse control methods. This is likely due to the fact that there are still no readily available software packages that enable ℓ_1 controllers to be solved conveniently. Hence, users are left with the non-trivial task of writing their own ℓ_1 controller synthesis software tools. Ultimately, the problem becomes an infinite dimensional linear programming problem which grows as the optimization progresses. As a result, use of the ℓ_1 controller initially becomes a research problem in itself rather than an easily usable control design tool.

The various approaches differ in terms of how easy each type of controller is to design. The PID controller is the most intuitive and quick to design and implement, but yields lower performance than the other techniques. As AFM users are well aware, PID control performance is also not robust. Model-inverse based controllers are straightforward to design once the inversion method is chosen. However, depending on the plant and performance requirements, the designer should consider various model-inverse techniques in order to choose one that leads to the best performance. Although potentially effective, H_∞ control requires designers to select weighting functions based upon the plant uncertainty and desired performance. Due to the high sensitivity of the performance as a function of the weights, as noted earlier, control designers often struggle with the choice of these weights before arriving at a controller that performs well. The effectiveness of ℓ_1 optimal controllers is still debated, but assuming a designer has access to a software tool for the synthesis of ℓ_1 controllers, s/he is still faced with the choice of weights similar to those in the H_∞ control design.

While the control methods overviewed have demonstrated some level of success in improving the speed and quality of AFM images, there are still many areas to explore:

- A better understanding of the advantages, disadvantages, and tradeoffs between the methods is still needed. Under what circumstances (model uncertainty, performance metrics, controller order constraints, ease of design) will certain methods be better?
- No truly MIMO algorithms have been developed and applied for controlling AFMs. While cross-coupling has been noted in AFMs, the effect of the cross-coupling terms has not been explored extensively in the AFM control literature. MIMO controllers for the full plant model in (4) should be developed and evaluated to determine the performance gains achievable.
- For the overall combined feedforward/feedback control approach shown in Fig. 2, a more thorough investigation of how best to jointly design the feedforward and feedback compensators warrants further study.
- Other feedforward/feedback architectures that have been used in other application areas [21], [22], [37] should be explored for AFMs. In particular, the reference signals X_d , Y_d , and \tilde{Z}_{c_d} in Fig. 2 can be prefiltered before

injection into the loop. For instance, a simple input shaping technique [33] combined with a PI controller has been shown to enable significantly faster AFM scan rates compared to using the PI controller alone [28]. Other prefiltering methods should be investigated for improving the speed and quality of AFM images.

- While robust control methods may provide practical controllers in the presence of model uncertainty, development of adaptive control methods for AFMs remains an open area that may provide enhanced performance. For instance, the repetitious nature of the raster (X - Y) scan motion could be used to add on-line adaptation to the control methods. On-line adaptation could also be investigated for the Z -motion control; assuming the topology of samples does not change dramatically from line to line, the "repetitive" information from the previous recorded scan line could be used for adapting and tuning the Z -motion controller in the current scan line. These adaptive methods will enable tuning and optimization of performance even as cantilever tips and samples are changed, as well as adapting to environmental changes and component drift.

In summary, the AFM is already recognized as an important tool for imaging nanoscale structures, and it is becoming a driving technology in nanomanipulation and nanoassembly. There are many areas for further investigation that can improve the control of AFMs significantly to enable an even wider range of applications throughout various disciplines.

REFERENCES

- [1] D. Y. Abramovitch, S. B. Andersson, L. Y. Pao, and G. Schitter. "A Tutorial on the Mechanisms, Dynamics, and Control of Atomic Force Microscopes," *Proc. Amer. Ctrl. Conf.*, July 2007.
- [2] S. B. Andersson and J. Park. "Tip Steering for Fast Imaging in AFM," *Proc. Amer. Ctrl. Conf.*, June 2005.
- [3] S. B. Andersson. "An Algorithm for Boundary Tracking in AFM," *Proc. Amer. Ctrl. Conf.*, June 2006.
- [4] S. B. Andersson and D. Y. Abramovitch. "A Survey of Non-Raster Scan Methods with Application to Atomic Force Microscopy," *Proc. Amer. Ctrl. Conf.*, July 2007.
- [5] T. Ando, N. Kodera, E. Takai, D. Maruyama, K. Saito, and A. Toda. "A High-Speed Atomic Force Microscope for Studying Biological Macromolecules," *Proc. Nat. Acad. Sci.*, 2001.
- [6] K. J. Åström and T. Hägglund. *Advanced PID Control*, ISA Press, 2005.
- [7] G. K. Binnig and D. Smith. "Single-Tube Three Dimensional Scanner for Scanning Tunneling Microscopy," *Rev. Sci. Instr.*, Mar. 1986.
- [8] D. Croft and S. Devasia. "Vibration Compensation for High Speed Scanning Tunneling Microscopy," *Rev. Sci. Instr.*, Dec. 1999.
- [9] D. Croft, G. Shed, S. Devasia. "Creep, Hysteresis, and Vibration Compensation for Piezoactuators: Atomic Force Microscopy Application," *ASME J. Dyn. Sys., Meas., & Ctrl.*, Mar. 2001.
- [10] F. El Feninat, T. H. Ellis, E. Sacher, I. Stangel. "A Tapping Mode AFM Study of Collapse and Denaturation in Dentine Collagen," *Dental Materials*, 2001.
- [11] O. M. El Rifai and K. Youcef-Toumi. "Design and Control of Atomic Force Microscopes," *Proc. Amer. Ctrl. Conf.*, June 2003.
- [12] A. Engel, H. E. Gaub, and D. Müller. "Atomic Force Microscopy: A Forceful Way with Single Molecules," *Current Biology*, Feb. 1999.
- [13] K. Glover and D. McFarlane. "Robust Stabilization of Normalized Co-Prime Factor Plant Descriptions with H_∞ -Bounded Uncertainty," *IEEE Trans. Auto. Ctrl.*, Aug. 1989.
- [14] N. Kodera, H. Yamashita, and T. Ando. "Active Damping of the Scanner for High-Speed Atomic Force Microscopy," *Rev. Sci. Instr.*, May 2005.
- [15] N. Kodera, M. Sakashita, and T. Ando. "Dynamic Proportional-Integral-Differential Controller for High-Speed Atomic Force Microscopy," *Rev. Sci. Instr.*, Aug. 2006.
- [16] J. Kwon, J. Hong, Y.-S. Kim, D.-Y. Lee, K. Lee, S. Lee, and S. Park. "Atomic Force Microscope with Improved Scan Accuracy, Scan Speed, and Optical Vision," *Rev. Sci. Instr.*, Oct. 2003.
- [17] D. McFarlane and K. Glover. "A Loop Shaping Design Procedure Using H_∞ Synthesis," *IEEE Trans. Auto. Ctrl.*, July 1992.
- [18] V. J. Morris, A. P. Gunning, and A. R. Kirby. *Atomic Force Microscopy for Biologists*, Imperial College Press, 1999.
- [19] B. Potsaid and J. T. Wen. "High Performance Motion Tracking Control," *Proc. IEEE Int. Conf. Ctrl. Appl.*, Sept. 2004.
- [20] J. M. Rieber, G. Schitter, A. Stemmer, and F. Allgöwer. "Experimental Application of ℓ_1 -Optimal Control in Atomic Force Microscopy," *Proc. IFAC World Cong.*, July 2005.
- [21] B. P. Rigney, L. Y. Pao, and D. A. Lawrence. "Settle-Time Performance Comparisons of Approximate Inversion Techniques for LTI Nonminimum Phase Systems," *Proc. Amer. Ctrl. Conf.*, June 2006.
- [22] B. P. Rigney, L. Y. Pao, and D. A. Lawrence. "Model Inversion Architectures for Settle Time Applications with Uncertainty," *Proc. IEEE Conf. Dec. & Ctrl.*, Dec. 2006.
- [23] S. M. Salapaka, A. Sebastian, J. P. Cleveland, and M. V. Salapaka. "High Bandwidth Nano-Positioner: A Robust Control Approach," *Rev. Sci. Instr.*, Sept. 2002.
- [24] S. M. Salapaka, T. De, and A. Sebastian. "A Robust Control Based Solution to the Sample-Profile Estimation Problem in Fast Atomic Force Microscopy," *Int. J. Robust & Nonlin. Ctrl.*, 2005.
- [25] G. Schitter, P. H. Menold, H. F. Knapp, F. Allgöwer, and A. Stemmer. "High Performance Feedback for Fast Scanning Atomic Force Microscopes," *Rev. Sci. Instr.*, Aug. 2001.
- [26] G. Schitter, R. W. Stark, and A. Stemmer. "Fast Contact-Mode Atomic Force Microscopy on Biological Specimen by Model-Based Control," *Ultramicroscopy*, 2004.
- [27] G. Schitter, R. W. Stark, and A. Stemmer. "Identification and Open-Loop Tracking Control of a Piezoelectric Tube Scanner for High-Speed Scanning-Probe Microscopy," *IEEE Trans. Ctrl. Sys. Tech.*, May 2004.
- [28] G. Schitter, G. E. Fantner, P. J. Thurner, J. Adams, and P. K. Hansma. "Design and Characterization of a Novel Scanner for High-Speed Atomic Force Microscopy," *Proc. IFAC Mech. Conf.*, Sept. 2006.
- [29] G. Schitter. "Advanced Mechanical Design and Control Methods for Atomic Force Microscopy in Real-Time," *Proc. Amer. Ctrl. Conf.*, July 2007.
- [30] A. Sebastian, M. V. Salapaka, and J. P. Cleveland. "Robust control approach to atomic force microscopy," *Proc. IEEE Conf. Dec. & Ctrl.*, Dec. 2003.
- [31] A. Sebastian and S. M. Salapaka. "Design Methodologies for Robust Nano-Positioning," *IEEE Trans. Ctrl. Sys. Tech.*, Nov. 2005.
- [32] Z. Shao, J. Mou, D. M. Czajkowsky, J. Yang, J.-Y. Yuan. "Biological Atomic Force Microscopy: What is Achieved and What is Needed," *Adv. in Physics*, 1996.
- [33] W. E. Singhose, W. P. Seering, and N. C. Singer. "Improving Repeatability of Coordinate Measuring Machines with Shaped Command Signals," *Precision Engr.*, 1996.
- [34] S. Skogestad and I. Postlethwaite. *Multivariable Feedback Control: Analysis and Design*, Wiley, 1996.
- [35] A. Stemmer, G. Schitter, J. M. Rieber, and F. Allgöwer. "Control Strategies Towards Faster Quantitative Imaging in Atomic Force Microscopy," *Euro. J. Ctrl.*, 2005.
- [36] S. Tien, Q. Zou, and S. Devasia. "Iterative Control of Dynamics-Coupling-Caused Errors in Piezoscanners During High-Speed AFM Operation," *IEEE Trans. Ctrl. Sys. Tech.*, Nov. 2005.
- [37] M. Tomizuka. "Zero Phase Error Tracking Algorithm for Digital Control," *ASME J. Dyn. Sys., Meas., & Ctrl.*, Mar. 1987.
- [38] J. T. Wen and B. Potsaid. "An Experimental Study of a High Performance Motion Control System," *Proc. Amer. Ctrl. Conf.*, June 2004.
- [39] Y. Wu and Q. Zou. "Iterative Control Approach to Compensate for the Hysteresis and the Vibrational Dynamics Effects of Piezo Actuators," *Proc. Amer. Ctrl. Conf.*, June 2006.
- [40] K. Zhou, J. C. Doyle, K. Glover. *Robust and Optimal Control*, Prentice-Hall, 1996.
- [41] Q. Zou and S. Devasia. "Preview-Based Optimal Inversion for Output Tracking: Application to Scanning Tunneling Microscopy," *IEEE Trans. Ctrl. Sys. Tech.*, May 2004.